PHYSICAL REVIEW B VOLUME 9, NUMBER 2 15 JANUARY 1974

Temperature and pressure dependence of the Si(222) forbidden reflection and the vibration of the bonding charge

Isao Fujimoto

Broadcasting Science Research Laboratories of Nippon Hoso Kyokai, 1-10-11 Kinuta, Setagaya-ku, Tokyo 157, Japan

(Received 18 September 1973)

The variation of the integrated intensities was measured between room temperature and 600 °C using a high-power x-ray generator. The pressure dependence was also measured up to 5.2 kbar and found to be so small that the implicit temperature dependence can be neglected. By making corrections for the effect of anharmonic vibration of nucleus using the neutron data obtained by Keating *et al.*, the temperature coefficient of the bonding-charge component of the structure factor was obtained to be $(0.90 \pm 0.10)M_c$, where M_c is the ordinary Debye-Waller factor with the Debye temperature of 540 °K. Simple calculation of the displacement of the bonding charge was made by assuming that the point bonding charges are always located at the midpoint between neighboring atoms. The ratio of the mean-square amplitude of the bonding charge to that of core was calculated to be 0.74 ± 0.05, which has a fairly good agreement with the value measured. Also the structure factor of the (222) reflection was obtained by the Pendellösung fringe method to be $1.50_5 \pm 0.015$ at 20 °C.

I. INTRODUCTION

Many theoretical studies on lattice dynamics of diamond-structure crystals have been made to understand the dielectric and optical properties. The rigid-ion model, where the outer electrons were assumed to move with the nucleus rigidly, could not explain the observed dispersion curves without postulating the interactions between at least fifth-nearest-neighbor atoms.[1] This difficulty was resolved[2] by applying the shell model where atoms were assumed to be polarizable in thermal motion. However, there remained the necessity of employing many parameters to fit the observed dispersion curves so that physical interpretation was difficult. On the other hand, Phillips[3] proposed an empirical theory for covalent bond where the simple relation between the magnitude of the point bonding charge at the midpoint of the covalent bond and the macroscopic dielectric constant was conjectured. His theory has been applied successfully to calculate various properties of many covalent crystals such as cohesive energy and nonlinear optical susceptibilities. The dielectric-screening theory[4] based on Phillips's bond-charge model has explained successfully the phonon dispersion curves of Si with one adjustable parameter.

In all the cases the comparison with experiment was made as to the phonon dispersion relations, i.e., main concern was about the motion of the core and there has been no direct experimental evidence for the motion of the outer valence electrons. As the weak (222) forbidden reflection of x rays in diamond-structure crystals[5–14] arises mainly from covalent bonding charges in contrast to normal Bragg reflections due mainly to the scattering by core electrons, the x-ray study on this forbidden reflection can be considered to provide a direct evidence for both the lattice-dynamics calculation and the Phillips bond-charge theory. There have been some conjectures[11,14] that the Debye-Waller factor for the (222) forbidden reflection should be much less than that expected from the ordinary formula because the bonding electrons can be considered to be relatively stationary according to the shell model. Recently, several authors[15] found that the x-ray structure factor of the (222) reflection of Si due to bonding electrons was less temperature dependent than that expected from ordinary Debye-Waller factor and took this as evidence in support of the shell model. However, detailed analyses based on phonon modes and phonon spectrum have not been made yet. Among many phonon modes, transverse-acoustic modes can be considered to predominate for the Debye-Waller factor because those modes have more vibrational amplitudes than other modes, and acoustic modes have a tendency to make bonding electrons to vibrate more or less together with core. Therefore, this consideration may lead to an anxiety that they might have found somewhat too much difference between both the Debye-Waller factors for the core and the bonding electrons.

In the present study a precise measurement for the (222) forbidden reflection of Si has been carried out with a high-power rotating-anode x-ray generator, because the (222) reflection intensities are extremely weak, and a simple calculation has been made to analyze the results.

II. THEORY

The effect of the lattice vibration on the distortion of the bonding-electron distribution is not clear. For the first approximation, we assume that the well localized bonding charges follow the vibration of cores in such a way that they are al-

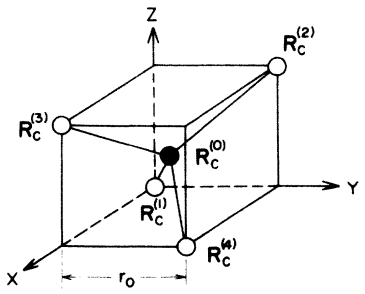

FIG. 1. Atoms of the diamond structure. Here $\frac{1}{8}$ of the cubic unit cell is shown. The black circles correspond to the atoms of A sites and the white circles correspond to those of B sites.

ways at the midpoint between neighboring cores. On this assumption the vibration of the bonding charge can be evaluated by the simple computation as follows.

A. Formulation

There are two kinds of sites, A and B, in the diamond lattice. When we take the A atom at $\vec{R}_c^{(0)}=\vec{R}$, the four-nearest-neighbor atoms on B sites are at $\vec{R}_c^{(s)}=\vec{R}+\vec{r}^{(s)}$, where $\vec{r}^{(s)}=(-1,-1,-1)\frac{1}{2}r_0$, $(-1,1,1)\frac{1}{2}r_0$, $(1,-1,1)\frac{1}{2}r_0$, $(1,1,-1)\frac{1}{2}r_0$ for $s=1, 2, 3, 4$, respectively, as shown in Fig. 1 taking the side of the cubic unit cell as $2r_0$. The bond-charge position $\vec{R}_b^{(s)}$ is given by

$$\vec{R}_b^{(s)}=\tfrac{1}{2}(\vec{R}_c^{(0)}+\vec{R}_c^{(s)}) \quad \text{for } s=1, 2, 3, 4, \tag{2.1}$$

and therefore the displacement of the bond-charge position $\vec{u}_b$ can be obtained from the displacement of core $\vec{u}_c$ as

$$\vec{u}_b^{(s)}=\tfrac{1}{2}(\vec{u}_c^{(0)}+\vec{u}_c^{(s)}) \quad \text{for } s=1, 2, 3, 4 \quad . \tag{2.2}$$

In the theory of lattice dynamics[16] the displacement of core for the phonon mode with wave vector $\vec{q}$ is given by

$$\vec{u}_c=\vec{U}_c(\vec{q})\, e^{i(\vec{q}\cdot\vec{r}-\omega t)} \quad , \tag{2.3}$$

so that Eq. (2.2) can be written

$$\vec{u}_b^{(s)}=\vec{U}_c^{(A)}\tfrac{1}{2}\{1+e^{i\phi^{(s)}}\}e^{i(\vec{q}\cdot\vec{R}-\omega t)} \quad , \tag{2.4}$$

where

$$\phi^{(s)}(\vec{q})=\vec{q}\cdot\vec{r}^{(s)}+\phi_c(\vec{q}) \tag{2.5}$$

and the relation

$$U_c^{(s)}/U_c^{(0)}\equiv U_c^{(B)}/U_c^{(A)}=e^{i\phi_c(\vec{q})} \tag{2.6}$$

was used, because the vibrational amplitude is equal for the two sites. From Eqs. (2.3) and (2.4),

$$|u_b^{(s)}|^2=b^{(s)}(\vec{q})|u_c|^2 \quad , \tag{2.7}$$

where

$$b^{(s)}(\vec{q})=|\tfrac{1}{2}(1+e^{i\phi^{(s)}(\vec{q})})|^2 =\tfrac{1}{2}[1+\cos\phi^{(s)}(\vec{q})] \quad ,$$

i.e., the square of the displacement of the bond-charge position is proportional of that of core. For each phonon mode, $b^{(s)}(\vec{q})$ is different for the four bond-charge positions. However, the average can be used because of cubic symmetry of the crystal, i.e.,

$$b(\vec{q})=\frac{1}{4}\sum_{s=1}^{4}b^{(s)}(\vec{q}) =\frac{1}{4}\sum_{s=1}^{4}\frac{1}{2}[1+\cos\phi^{(s)}(\vec{q})] \quad . \tag{2.9}$$

On the other hand, the decrease in the structure factor due to thermal vibration can be given by the Debye-Waller factor e^{-M}, i.e., for cubic crystals

$$M=\tfrac{1}{6}Q^2\langle u^2\rangle=\frac{\hbar}{12Nm}Q^2\sum_{j,\vec{q}}\frac{\coth[\frac{1}{2}\beta\hbar\omega_j(\vec{q})]}{\omega_j(\vec{q})} \quad , \tag{2.10}$$

where $\langle u^2\rangle$ is the mean-square displacement, $Q=4\pi\sin\theta/\lambda$, $\omega_j(\vec{q})$ is the circular frequency of jth phonon mode with wave vector $\vec{q}$, m is the mass of the atom, N is the number of unit cells in crystal, and $\beta=1/kT$. Combining Eqs. (2.7), (2.9), and (2.10) the ratio of the exponent of the Debye-Waller factor for the bonding charge M_b to that for the core M_c can be given by

$$\frac{M_b}{M_c}=\frac{\langle u_b^2\rangle}{\langle u_c^2\rangle} =\frac{\sum_{j,\vec{q}}b(\vec{q})\coth[\frac{1}{2}\beta\hbar\omega_j(\vec{q})]/\omega_j(\vec{q})}{\sum_{j,\vec{q}}\coth[\frac{1}{2}\beta\hbar\omega_j(\vec{q})]/\omega_j(\vec{q})} \quad . \tag{2.11}$$

In order to obtain M_b/M_c, $b(\vec{q})$ must be calculated for each phonon mode.

B. Calculation of $b(\vec{q})$ and M_b/M_c

To calculate $b(\vec{q})$, $\phi^{(s)}(\vec{q})$ must be obtained, i.e., the secular equation in lattice dynamics must be solved. For simplicity, an approximation is made that the vibration of core can be well described by Cochran's theory[2] which gives a good interpretation to the observed phonon dispersion curves of Ge. The results for Ge are applicable for Si because the two materials can be considered to be homologous as to lattice vibration.[17]

After Cochran[2] for the phonon modes with wave vector $\vec{q}$ in symmetry directions [100] and [111],

$$U_c^{(B)}/U_c^{(A)}=\pm|A|/A=\pm e^{-i\phi_A} \quad , \tag{2.12}$$

where the + and − signs refer to optic and acoustic modes, respectively, and A is the coefficient of interaction between polarizable atoms. From Eqs.

(2.6) and (2.12),

$$\phi_c(\vec{q}) = -\phi_A(\vec{q}) \quad \text{for optic mode,}$$

$$= -\phi_A(\vec{q}) + \pi \quad \text{for acoustic mode.} \tag{2.13}$$

From Eqs. (2.5), (2.9), and (2.13), $b(\text{optic}) + b(\text{acoustic}) = 1$ for the same wave vector $\vec{q}$, and therefore only the acoustic modes are concerned in the following computation of $b(\vec{q})$. As the computation of $\phi_A(\vec{q})$ is rather complicated using many parameters, $\phi_R (= \phi_T = \phi_S)$ in the notation of Cochran's paper[2] can be used for $\phi_A(\vec{q})$ within an error of less than 1% in the resultant ratio M_b/M_c. In this approximation $\phi^{(s)}(\vec{q})$ can be given for the phonon modes with wave vector $\vec{q}$ in symmetry directions [100] and [111] as follows: For the [100] direction $\vec{q} = (\zeta, 0, 0)$, where ζ ranges from 0 to 1 so that $\theta = \frac{1}{2}\zeta\pi_0$ ranges from 0 to $\frac{1}{2}\pi$, and for the [111] direction $\vec{q} = (\zeta, \zeta, \zeta)$, where ζ ranges from 0 to $\frac{1}{2}$ so that θ from 0 to $\frac{1}{4}\pi$:

[100] transverse-acoustic mode:

$$\phi^{(s)}(\vec{q}) = \pm\theta - \tan^{-1}(-\gamma_R \tan\theta) \quad , \tag{2.14}$$

[100] longitudinal-acoustic mode:

$$\phi^{(s)}(\vec{q}) = \pm\theta \quad , \tag{2.15}$$

where the + and − signs are taken for the sites with $s = 3, 4$ and $s = 1, 2$, respectively.

[111] transverse-acoustic mode:

$$\phi^{(s)}(\vec{q}) = -3\theta - \tan^{-1}\left(\frac{\gamma_R + \tan^2\theta}{1 + \gamma_R \tan^2\theta} \tan\theta\right) \quad \text{for } s = 1 \ ,$$

$$= \theta - \tan^{-1}\left(\frac{\gamma_R + \tan^2\theta}{1 + \gamma_R \tan^2\theta} \tan\theta\right) \quad \text{for } s = 2, 3, 4; \tag{2.16}$$

[111] longitudinal-acoustic mode:

$$\phi^{(s)}(\vec{q}) = -3\theta - \tan^{-1}\left(\frac{\tan^2\theta - 2\gamma_R}{1 - 2\gamma_R \tan^2\theta} \tan\theta\right) \quad \text{for } s = 1 \ ,$$

$$= \theta - \tan^{-1}\left(\frac{\tan^2\theta - 2\gamma_R}{1 - 2\gamma_R \tan^2\theta} \tan\theta\right) \quad \text{for } s = 2, 3, 4 \ . \tag{2.17}$$

Here γ_R is the certain ratio of the force constants; Cochran took this value to be 0.69 from the experimental values of elastic constants. On the other hand Dolling[18] took this value of γ_R to be 0.21 on the modified shell model introducing the short-range interactions between second-nearest neighbors. For both cases with so much different values of γ_R, $b(\vec{q})$ was calculated from Eqs. (2.14)–(2.17), and shown in Fig. 2 together with optic modes. As can be seen from Fig. 2, only $b(\vec{q})$ for longitudinal modes in [111] direction is sensitive to the value of γ_R and $b(\vec{q})$ for other modes is not much affected by the value of γ_R. In order to evaluate M_b/M_c, $b(\vec{q})$ must be averaged over all phonon modes in the first Brillouin zone. This average was approximated with the weighted average in the direction of [100] and [111].

For the evaluation of Eq. (2.11) the sum can be replaced by integrals. In taking the average in one direction with definite solid angle in $\vec{q}$ space the densities of phonon mode is proportional to q^2, i.e., $d\vec{q} \propto q^2\, dq$ with the number of the transverse mode twice that of longitudinal mode. By using the multiplicity factor of 6 and 8 for $\langle 100 \rangle$ and $\langle 111 \rangle$ direction each, we finally obtain the ratio M_b/M_c:

$$\frac{M_b}{M_c} = \left(6\int_{\langle 100\rangle} b(\vec{q}) \frac{\coth\left[\frac{1}{2}\beta\hbar\omega(\vec{q})\right]}{\omega(\vec{q})} q^2\, dq + 8\int_{\langle 111\rangle} b(\vec{q}) \frac{\coth\left[\frac{1}{2}\beta\hbar\omega(\vec{q})\right]}{\omega(\vec{q})} q^2\, dq\right)$$

$$\times\left(6\int_{\langle 100\rangle} \frac{\coth\left[\frac{1}{2}\beta\hbar\omega(\vec{q})\right]}{\omega(\vec{q})} q^2\, dq + 8\int_{\langle 111\rangle} \frac{\coth\left[\frac{1}{2}\beta\hbar\omega(\vec{q})\right]}{\omega(\vec{q})} q^2\, dq\right)^{-1} \ . \tag{2.18}$$

The value $W(\vec{q}) \equiv q^2 \coth\left[\frac{1}{2}\beta\hbar\omega(\vec{q})\right]/\omega(\vec{q})$ was calculated in the [100] and [111] directions using the experimental phonon dispersion curves obtained by Dolling[18] and shown in Fig. 3. As can be seen from the curves, the transverse-acoustic modes predominate in the above average. Thus, the value of M_b/M_c was obtained to be 0.73 ± 0.05 taking $\gamma_R = 0.69$. The change of the value of the parameter γ_R does not produce perceptible changes in the result because the transverse-acoustic modes which are a dominant part in the calculation of M_b/M_c are not sensitive to the value of γ_R. For $\gamma_R = 0.21$, for example, the value of M_b/M_c was obtained to be 0.74 ± 0.05.

III. EXPERIMENTAL

Sample crystals used were cut from a pure and dislocation-free crystal grown by the floating-zone method in vaccum. They were lapped by 1000-grit powder and etched in a 4:1:1 volume parts HNO_3-HF-CH_3COOH solution to remove the surface damage. For the measurement of the temperature dependence, specimens were heated up to 600 °C in an evacuated furnace which is shown schematically in Fig. 4. The furnace was designed so as not to induce thermal strains in the specimen crystal. The crystal temperature was measured by both platinum–platinum-13-at.% rhodium and Chromel-

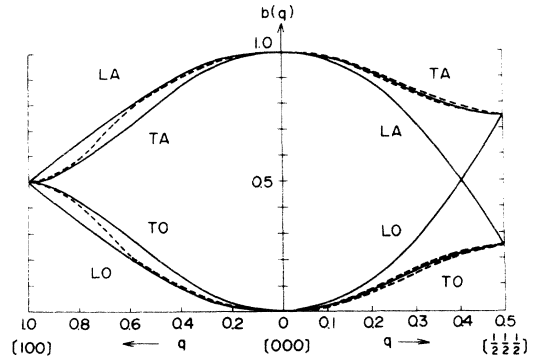

FIG. 2. Calculated ratio of the square amplitude of the vibration of the bonding charge position to that of core for the phonon mode with wave vector $\vec{q}$ in [100] and [111] directions. The solid line is the value with $\gamma_R = 0.69$ and the broken line with $\gamma_R = 0.21$. The longitudinal modes with $\vec{q}$ in the [100] direction do not depend on γ_R.

Alumel thermocouples which were placed close to the specimen at different positions. For the measurement of pressure dependence, a clamped-type high-pressure bomb was designed for x-ray diffraction experiment as shown in Fig. 5. A tapered beryllium bomb with a diameter of 20 mm was placed at the center of the vessel, which worked as windows for the x-ray beams and served to hold the specimen and to retain the pressure. Hydrostatic pressure was produced via n-petane transmission medium by driving a piston by a hydraulic press and clamped by a locking nut. The pressure was calibrated using the phase transition of ammonium fluoride NH_4F at 3.65 kbar at room temperature.

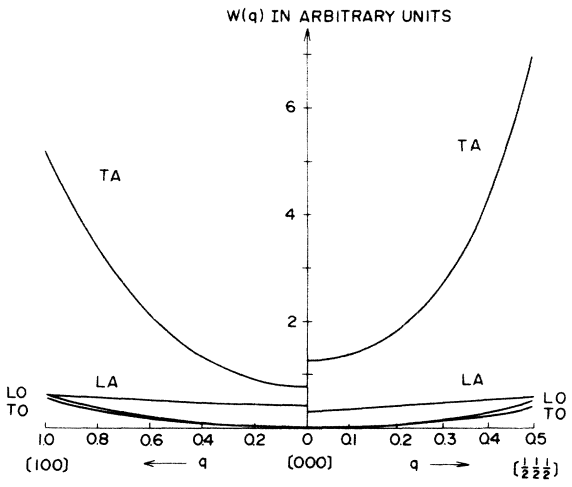

FIG. 3. Calculated value of the weight $W(\vec{q}) = q^2 \times \coth[\frac{1}{2}\beta\hbar\omega(\vec{q})]/\omega(\vec{q})$. For the calculation of M_b/M_c in the text the value for the transverse modes shown here must be multiplied by 2.

A rotating-anode x-ray generator was operated at 50 KV 400 mA, and the x-ray beam was monochromatized by the (111) reflection of a Si perfect crystal. A scintillation counter with a pulse-height analyzer was employed. The integrated intensity for the (222) reflection was measured in the Bragg case with Ag$K\alpha_1$ and Cu$K\alpha_1$ radiations, in the Laue case with Ag$K\alpha_1$ and also for (333) reflection in the Bragg case with Ag$K\alpha_1$ by rotating the furnace or pressure bomb using the folded-lever arrangement driven by precision micrometer. Typical rocking curve for the (222) forbidden reflection is shown in Fig. 6. The integration range for the (222) reflection was taken to be 5.3′ of arc with Ag$K\alpha_1$ and 7.1′ of arc with Cu$K\alpha_1$. Several run at each time was made and an average was taken, and the intensities were confirmed to have the same value within an experimental error before and after the high-temperature or high-pressure measurement. The peak intensity of the (222) reflection was about 2500 counts/sec and the total counts were about 5×10^4.

For such a weak reflection as the forbidden reflection the effect of simultaneous reflections can not be neglected,[19] and their positions in azimuthal angle together with indices have been shown by Cole *et al.*[20] The experimental Umweganregung pattern in Si was obtained using Cu$K\alpha_1$ and Ag$K\alpha_1$ radiation and shown in Fig. 7. To avoid this effect, the fine adjustment in azimuthal angle was made by the screw shown in Fig. 4, and the incident beam with a narrow vertical divergence of about 0.5° was used. The positions in azimuthal angle at which the measurement were made are shown by the arrows in Fig. 7. The photographs taken at

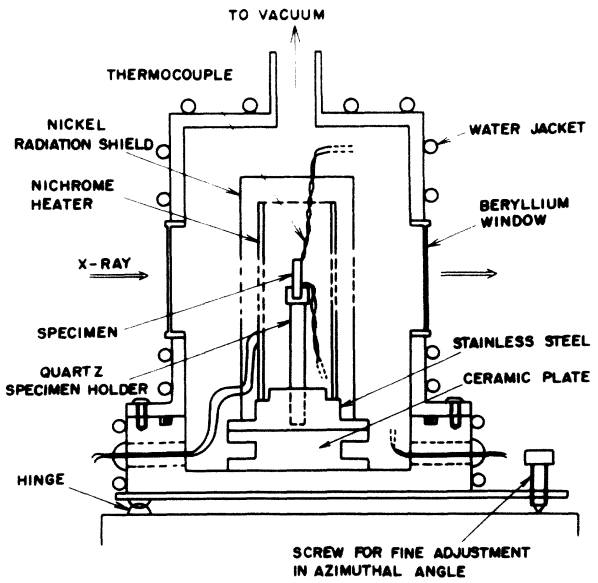

FIG. 4. Schematic view of the furnace.

those positions never showed any pattern due to the simultaneous diffraction. As the Umweganregung pattern varies with lattice parameter, it was confirmed that the crystal was still positioned freely from Umweganregung effect in all the temperature and pressure ranges of the measurement. Although the Umweganregung may occur easily for Ag$K\alpha_1$ radiation because its Ewald sphere is larger compared with the Cu$K\alpha_1$ -radiation case, the intensity ratio of the simultaneous diffraction to the true (222) reflection is smaller, as can be seen in Fig. 7, because the absorption is much less for the large extinction distance of the (222) reflection. The comparison with the data obtained by Cu$K\alpha_1$ showed that the intensity of the simultaneous reflections can be considered to be negligibly small even if they exist at the observed position though it seems unexpected from the estimation by Prager.[21]

Dynamical equation was used to obtain the structure factor at each temperature or pressure, and small corrections were made for the change in both the Bragg angle and the volume of the unit cell due to thermal expansion or due to the compression by high pressure. The absolute value of F_{222} at room temperature and 1-atm pressure was measured precisely both by the Pendellösung method and by the integrated-intensity method.

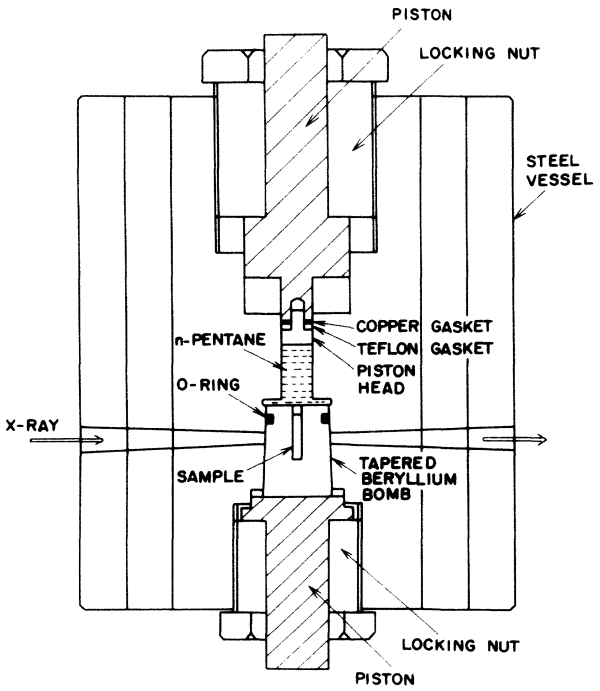

FIG. 5. Schematic view of the high-pressure bomb.

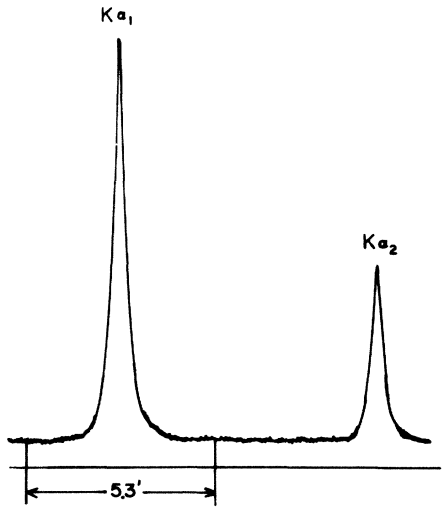

FIG. 6. Rocking curve of the 222 forbidden reflection together with integration range.

IV. ABSOLUTE MEASUREMENT OF THE STRUCTURE FACTOR OF (222) FORBIDDEN REFLECTION

Many authors have reported the experimental value of F_{222} by the integrated intensity methods, which ranges from 0.90 to 1.78.[6,7,9,10,13,14,22] Recently, absolute measurement of the structure factor with high accuracy by the Pendellösung fringe method have been reported by Hattori *et al.*,[23] but not made for the forbidden reflection, probably because the reflection is so weak. Here the structure factor of the forbidden reflection was measured by the Pendellösung fringe method using the high-power x-ray generator and compared with the one obtained by the measurement of integrated intensity relative to (333) reflection.

A. Pendellösung fringe method

Wedge-shaped crystals were prepared with wedge angle of about 45°. Section topographs were taken in symmetric Laue case with Ag$K\alpha_1$ radiation operated at 50 KV, 400 mA with exposure time of about 12 h. Typical topograph is shown in Fig. 8(a) and the first-fringe maximum can be clearly seen. A photometry trace was made along the center of the x-ray fan on the nuclear plate and is shown in Fig. 8(b). The crystal thickness for the first minimum and maximum of the fringes was measured to be $1.65_6 \pm 0.01$ mm and $2.46_0 \pm 0.01$ mm, respectively. According to dynamical theory of x-ray diffraction due to spherical waves,[24] the diffracted intensities along the net plane through the incident position in the section topograph are given by

$$I_g = \frac{1}{32\pi}\,\frac{1}{K\gamma}\,\exp[-(\mu_0/\cos\theta_B)l]\,|\bar{\beta}|^2$$

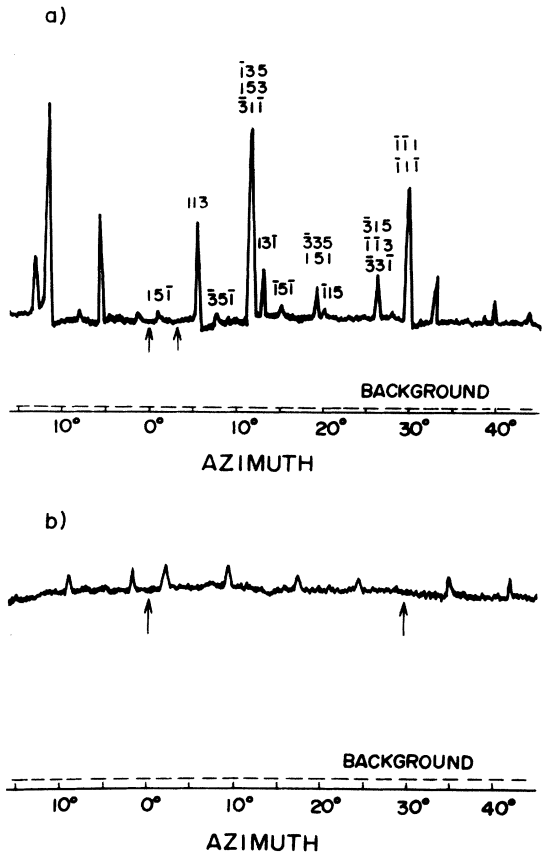

FIG. 7. Umweganregung pattern at (222) position in silicon; (a) using Cu$K\alpha_1$ radiation, (b) using Ag$K\alpha_1$ radiation. The zero of the azimuth was chosen with a [110] axis lying on both the (222) lattice plane and the diffraction plane. The positions in azimuth used are shown by the arrows.

$$\times \left| J_0(l\bar{\beta}\sin\theta_B)\right|^2 \quad . \tag{4.1}$$

Here K is the wave vector, μ_0 is the linear absorption coefficient, θ_B is the Bragg angle, l is the distance along the net plane, J_0 is the zeroth-order Bessel function, $\bar{\beta} = (\chi_g\chi_{-g})^{1/2} KC/\sin 2\theta_B$, χ_g is the gth Fourier coefficient of the polarizability of the crystal for x rays, where C is the polarization factor, χ_g is related to structure factor F_g by

$$\chi_g = -(e^2\lambda^2/\pi mc^2 v) F_g \ ,$$

For the forbidden reflection the imaginary part of χ_g can be considered to be so small compared with the real part that we neglect the imaginary part of $\bar{\beta}$. The intensity minimum and maximum positions can be given from $dI_g/dl = 0$ and after some algebra

$$J_0(u) = 0 \quad \text{for minimum position} \quad , \tag{4.2}$$

$$\kappa_0 J_0(u) + J_1(u) = 0 \quad \text{for maximum position} \quad , \tag{4.3}$$

where $u = l\bar{\beta}\sin\theta_B$ and $\kappa_0 = \mu_0 l/2u\cos\theta_B$. The structure factor of the (222) forbidden reflection $|F_{222}|$ was calculated to be 1.50 ± 0.01 and 1.51 ± 0.01, each from the observed positions of the first minimum and maximum, respectively, using the above equations and the measured linear absorption coefficient of 7.15 cm^{-1}. The two values agree with each other within an experimental error and the average value of $1.50_5 \pm 0.015$ was obtained for $|F_{222}|$.

B. Integrated intensity measurement

Integrated intensities of (222) and (333) reflections were measured in symmetric Bragg case with Ag$K\alpha_1$ and Cu$K\alpha_1$ radiations. For the (333) reflec-

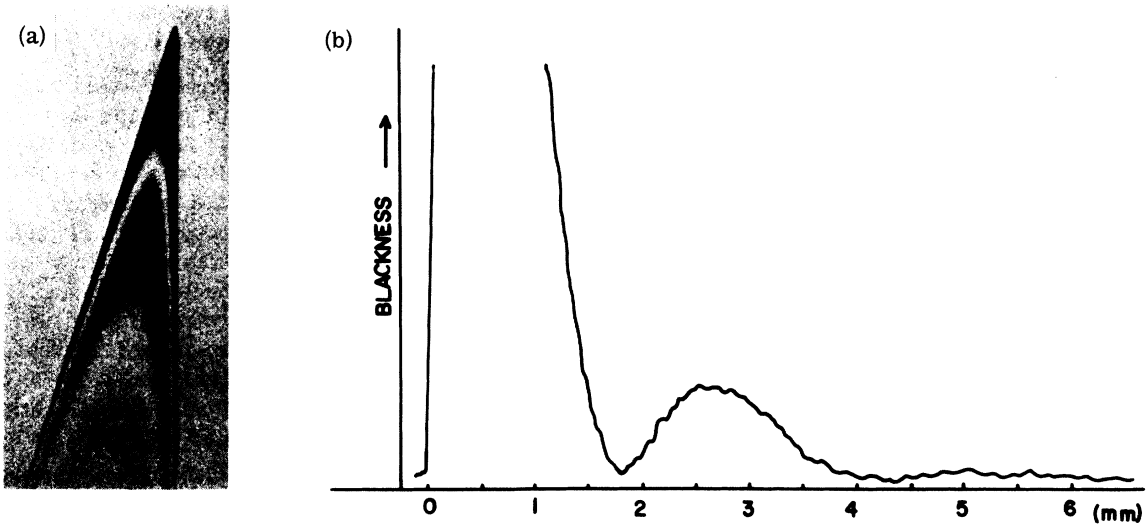

FIG. 8. (a) Photograph of the Pendelösung fringes in the section pattern of the (222) reflection. (b) The photometry curve of the plate (a) along the centre of the x-ray fan.

tion the reflected intensity was attenuated to be sufficiently low with absorbers so that the dead time corrections for the detector might be negligible. The dynamical equation was used for the integrated intensities,

$$I=\frac{C\lambda^2(e^2/mc^2)\,|F_H'|\,e^{-M}}{\pi V \sin 2\theta_B} R_H^y(\text{Bragg}) \quad , \qquad (4.4)$$

where I is the relative integrated intensity, C is the polarization factor, V is the volume of the unit cell, $|F_H'|$ is the real part of the structure factor, e^{-M} is the Debye-Waller factor, R_H^y(Bragg) is the absorption factor, and θ_B is the Bragg angle. The polarization factor was corrected for the monochromatized incident beam. Thermal-diffuse-scattering (TDS) correction was not made because the integration range was sufficiently small. Thus, the structure factor of the (222) forbidden reflection was obtained to be 1.51 ± 0.02 with Ag$K\alpha_1$ and 1.48 ± 0.02 with Cu$K\alpha_1$ from the measured intensity ratio of the (222) and (333) reflections, where Ag$K\alpha_1$ value of 33.03 obtained by Tanemura and Kato[25] by the Pendellösung method and Cu$K\alpha_1$ value of 34.05 reduced from it assuming Cromer's values[26] as the dispersion correction were used for the structure factor of (333) reflection. It should be noted that the values obtained both by the Pendellösung and integrated-intensity methods agree within the experimental error. The integrated-intensity method can be concluded to provide with a high accuracy similar to that obtained by the Pendellösung method and, therefore, was employed for the temperature- and pressure-dependence measurement because of more facilities in the experiment.

V. TEMPERATURE DEPENDENCE OF F_{bond}

Though the x-ray forbidden reflection has been known to arise mainly from sp^3 hybridized valence-electron charge distribution, the anharmonic vibration of nucleus also causes antisymmetric charge distribution around the equilibrium position of nucleus and acts against the antisymmetric bonding charge distribution, i.e.,

$$F_{222}=F_{\text{bond}}-F_{\text{anh}} \quad . \qquad (5.1)$$

This anharmonic part cannot be neglected, though small, for the temperature-dependence measurement. Dawson and Willis[27] formulated quantitatively this effect of anharmonic vibration of nucleus consistent with tetrahedral site symmetry. Using their formulation, Keating *et al.*[15] obtained the anharmonic component F_{anh} by neutron diffraction study. Therefore, F_{bond} can be obtained from F_{222} measured by the x-ray diffraction study using the Keating *et al.* results for F_{anh}.

The temperature dependence of F_{bond} can be considered to come from the implicit and explicit effects which are due to thermal dilation and lattice vibration, respectively. The implicit effect is negligibly small for normal reflections which arise mostly from the scattering by core electrons. For the forbidden reflection due mainly to outer valence electrons, however, the implicit effect can be appreciable, because the valence electron distribution may be changed with the variation of atomic distance as known from some properties such as energy gap and dielectric constant. The variation of F_{bond} with the lattice parameter can be measured by applying hydrostatic pressure to the crystals at a constant temperature. Using the variation measured, we can finally obtain the temperature variation of F_{bond} due to pure lattice vibration.

Temperature dependence of the structure factor of the (222) forbidden reflection was obtained in the range of 20–600 °C by the integrated-intensity method. Also the temperature dependence of the integrated intensity of the (333) reflection was measured to obtain the Debye temperature for Si and to check the accuracy of the experimental procedures. The results are shown in Fig. 9. From the temperature dependence of the (333) reflection, the Debye temperature was obtained to be (540 ± 20) °K in good agreement with the value reported by Batterman[28] and by Hattori *et al.*[23] Al-

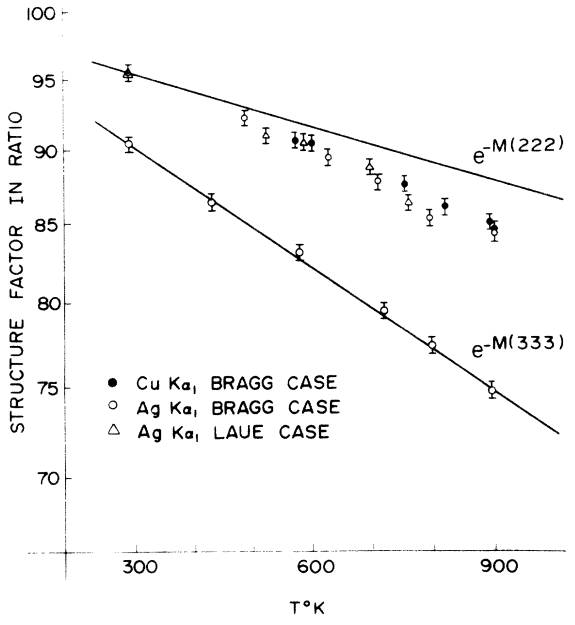

FIG. 9. Log structure factor vs reduced temperature $T[\phi(x)+\frac{1}{4}x]$ for (222) and (333) reflections in silicon. The solid line denotes the temperature variation assuming ordinary Debye-Waller factor with Debye temperature of 540 °K.

though there remains some discrepancies between the results obtained by Ag$K\alpha_1$ and Cu$K\alpha_1$ radiation, as can be seen in Fig. 9, the structure factor of the (222) forbidden reflection decreases more rapidly with temperature than that expected from ordinary Debye-Waller factor with the Debye temperature obtained above, and even more rapidly than that observed by Robert and Batterman.[22]

The pressure dependence of the structure factor of (222) reflection was measured up to 5.2 kbar at which the variation in the lattice constant has a magnitude similar to that of the lattice dilation at a temperature increase from 20 to 600 °C. Small corrections were made for the change in the absorption of the x rays by both the specimen crystal and the pressure transmission medium due to pressure variation. The variation of the structure factor F_{222} was found to be less than 0.3% with an experimental uncertainty of about 0.3%. This result shows that the implicit effect on the temperature dependence of the bonding electron distributions is very small and the dominant part is the explicit effect due to lattice vibration.

Using the above results of the temperature and pressure dependence of F_{222} and the neutron data of F_{anh} obtained by Keating *et al.*[15] the explicit temperature dependence of F_{bond} was obtained from the Eq. (5.1) and shown in Fig. 10. As can be seen in Fig. 10, the temperature variation of F_{bond} is less than the variation e^{-M_c} (solid line) expected from the rigid-ion model with a Debye temperature of 540 °K. By assuming e^{-M_b} behavior for the explicit temperature variation of F_{bond}, M_b was obtained to be $(0.85 \pm 0.05)M_c$ by Cu$K\alpha_1$ and $(0.95 \pm 0.05)M_c$ by Ag$K\alpha_1$. The theoretical temperature variation with $M_b = 0.74\ M_c$ is also shown by the broken line in Fig. 10.

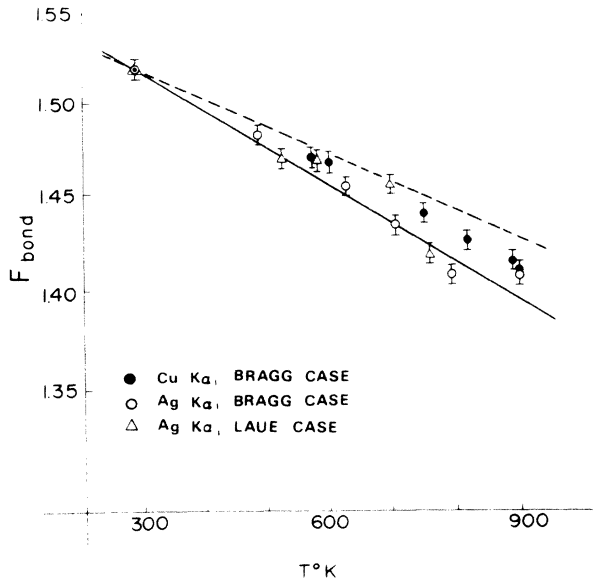

FIG. 10. Explicit temperature dependence of the structure factor of the (222) reflection. The solid line denotes the expected variation of F_{bond} on the basis of the rigid-ion model, i.e., $F_{bond} \sim e^{-M_c}$. The broken line is the calculated variation of F_{bond}, i.e., $F_{bond} \sim e^{-0.74M_c}$.

VI. DISCUSSION

The observed temperature variation of F_{bond} was found to be larger than that reported by Keating *et al.*[15] Though they did not take the implicit effect into account, the effect was found to be so small in the present study that it does not affect their results so much, and the origin of the difference between the two results is not clear.

The agreement between the observed results and the theoretical one made in the present study is fairly good though the former is more or less larger than the latter. In the calculation of M_b/M_c the bonding charge was assumed to be point charge situated at the midpoint of the bond but the real bonding charge can be considered to be not so much localized and to have some distributions along the bond connecting the nearest-neighbor atoms and as the bonding charge close to the nucleus follows the nucleus more closely than that at the midpoint, M_b/M_c may be somewhat larger than the above calculated value, which has favourable trend for the explanation of the observed one.

Another possible interpretation was examined for some of other theoretical calculations. The calculation of M_b/M_c by the direct computation of the displacement of the spherical shell $U(3)$ or $U(4)$ in Cochran's shell model[2] using the same parameter as he obtained was not found to work well because the displacement of the shell $U(3)$ or $U(4)$ was calculated to be larger than that of core $U(1)$ or $U(2)$ for the phonon mode with wave vector $\vec{q}$ in $\langle 111 \rangle$ direction, which may be difficult to justify physically. Though on the basis of bond charge theory, Phillips[29] interpreted the experimental results of the temperature dependence of F_{bond} obtained by Keating *et al.* by the observed temperature coefficient of refractive index, it does not fit the present results as described above. It should be mentioned here that Yu and Cardona[30] calculated the temperature coefficient of dielectric constant by the pseudopotential method after the Phillips model and when their results are rewritten in terms of Debye-Waller factor, the temperature coefficient in close to $e^{-4M(111)} = e^{-M(222)}$. When this calculated coefficient, though larger than that obtained from the experimental temperature coefficient of the refractive index, is used in the Phillips bond charge theory, we have $M_b/M_c \simeq 1$, which is rather close to the observed temperature dependence of F_{bond} obtained here. On the basis of this dielectric theory, however, it can be deduced that

the temperature dependences of the bonding-charge components of the various (hkl) $(h+k+l=4n+2)$ forbidden reflections do not depend on the reflection indices (hkl) which might seem rather unprobable.

VII. CONCLUSION

Simple expectation that the temperature dependence of the bonding-charge component of the forbidden reflection should be much less than that expected from the ordinary Debye-Waller factor considering that the outer valence electrons are relatively stationary seems to be not valid, and the observed results have shown that the temperature dependence is relatively large, i.e., the ratio of the mean-square amplitude of the vibration of the bonding electrons to that of the core obtained is 0.90 ± 0.10, which can be interpreted fairly well by the simple model. The results obtained above for the vibration of the bonding charge may be useful for the understanding of the dielectric and optical properties of other covalent crystals.

ACKNOWLEDGMENTS

The author wishes to thank Dr. J. Chikawa for helpful discussions and Dr. T. Abe for supplying silicon crystals. He also wishes to thank Dr. S. Imamura for the encouragement through this work.

[1]F. Herman, J. Phys. Chem. Solids 8, 405 (1959).
[2]W. Cochran, Proc. R. Soc. A 253, 260 (1959).
[3]J. C. Phillips, Phys. Rev. 166, 832 (1968); Phys. Rev. 168, 905 (1968).
[4]R. M. Martin, Phys. Rev. 186, 871 (1969).
[5]P. P. Ewald and H. Hönl, Ann. Phys. (N. Y.) 25, 281 (1936); Ann. Phys. (N. Y.) 26, 673 (1936).
[6]M. Renninger, Z. Kristallogr. 97, 107 (1937); Acta Crystallogr. 8, 606 (1955); Z. Kristallogr. 113, 99 (1960).
[7]S. Göttlicher and E. Wölfel, Z. Elektrochem. 63, 891 (1959).
[8]R. Brill, Acta Crystallogr. 13, 275 (1960).
[9]J. J. DeMarco and R. J. Weiss, Phys. Rev. 137, A1869 (1965).
[10]R. Collela and A. Merlini, Phys. Status Solidi 18, 157 (1966).
[11]R. J. Weiss, *X-ray Determination of Electron Distributions* (North-Holland, Amsterdam, 1966), p. 141.
[12]B. Dawson, Proc. R. Soc. A 298, 255 (1967); Proc. R. Soc. A 298, 379 (1967).
[13]A. W. Hewat *et al.*, Acta Crystallogr. A 25, S 213 (1969).
[14]L. D. Jennings, J. Appl. Phys. 40, 5038 (1969).
[15]D. Keating *et al.*, Phys. Rev. Lett. 27, 320 (1971); Phys. Rev. B 4, 2472 (1971).
[16]M. Born and K. Huang, *Dynamical Theory of Crystal Lattices* (Oxford U. P., Oxford, 1954).
[17]G. Dolling and A. D. B. Woods, in *Thermal Neutron Scattering*, edited by P. A. Egelstaff (Academic, London, 1965) p. 193.
[18]G. Dolling, in *Inelastic Scattering of Neutrons in Solids and Liquids* (IAEA, Vienna, 1963), p. 37.
[19]M. Renninger, Z. Phys. 106, 141 (1937).
[20]H. Cole, F. W. Chambers, and H. M. Dunn, Acta Crystallogr. 15, 138 (1962).
[21]P. R. Prager, Acta Crystallogr. A 27, 563 (1971).
[22]J. B. Roberto and B. W. Batterman, Phys. Rev. B 2, 3220 (1970).
[23]H. Hattori *et al.*, J. Phys. Soc. Jap. 20, 988 (1965).
[24]N. Kato, J. Appl. Phys. 39, 2225 (1968).
[25]S. Tanemura and N. Kato, Acta Crystallogr. A 28, 69 (1972).
[26]D. T. Cromer, Acta Crystallogr. 18, 17 (1965).
[27]B. Dawson and B. T. M. Willis, Proc. R. Soc. A 298, 307 (1967).
[28]B. W. Batterman, Phys. Rev. 127, 686 (1962).
[29]J. C. Phillips, Phys. Lett. A 37, 434 (1971).
[30]P. Y. Yu and M. Cardona, Phys. Rev. B 2, 3193 (1970).

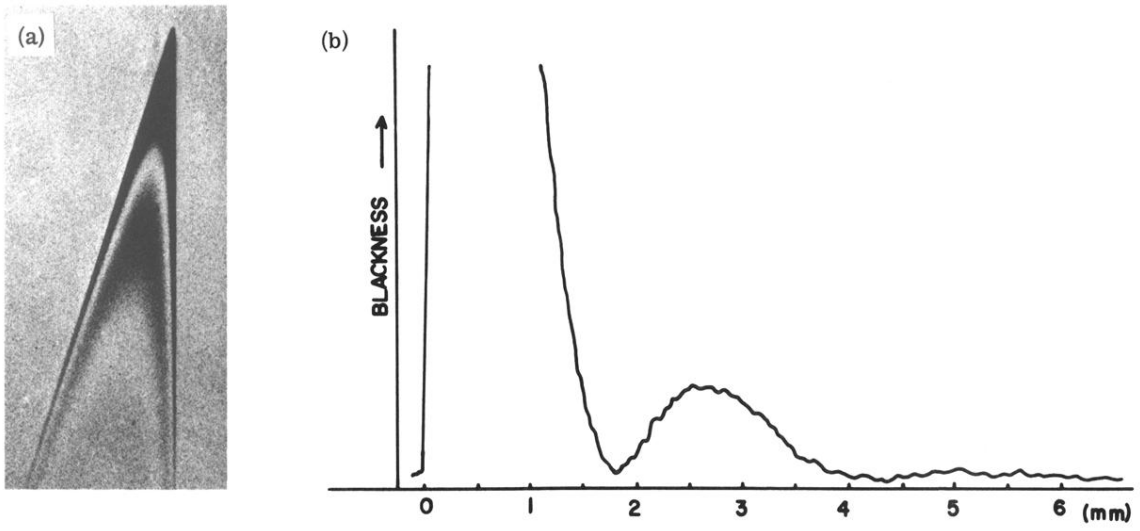

FIG. 8. (a) Photograph of the Pendelösung fringes in the section pattern of the (222) reflection. (b) The photometry curve of the plate (a) along the centre of the x-ray fan.